The Astrophysical Journal Letters, 908:L18 (7pp), 2021 February 10 https://doi.org/10.3847/2041-8213/abddb9

Lyα Irradiation of Superhydrogenated Coronene Films: Implications for H_2 Formation

V. Mennella[1], T. Suhasaria[1], L. Hornekær[2,3], J. D. Thrower[2,3], and G. Mulas[4,5]
[1] INAF–Osservatorio Astronomico di Capodimonte, via Moiariello 16, I-80131, Napoli, Italy; vito.mennella@inaf.it
[2] Department of Physics and Astronomy, Aarhus University, Ny Munkegade 120,DK-8000 Aarhus C, Denmark
[3] Center for Interstellar Catalysis, Aarhus University, Denmark
[4] INAF–Osservatorio Astronomico di Cagliari, Via della Scienza 5, I-09047 Selargius (CA), Italy
[5] Institut de Recherche en Astrophysique et Planètologie (IRAP), Université de Toulouse (UPS), CNRS, CNES, 9 Avenue du Colonel Roche, F-31028 Toulouse, France
Received 2020 November 3; revised 2021 January 15; accepted 2021 January 18; published 2021 February 15

Abstract

We present the results of an experimental study of the interaction of Lyα photons with superhydrogenated coronene films. The effects of ultraviolet (UV) irradiation have been analyzed with infrared spectroscopy. The spectral changes provide evidence for UV photodestruction of the C–D bonds of the superhydrogenated coronene with a cross section of $8 \pm 2 \times 10^{-20}$ cm^2. The comparison of our experimental result with the prediction from theoretical modeling suggests an extension of the region inside photodissociation regions where superhydrogenated coronene can survive and contribute to H_2 formation. H_2 formation through abstraction in superhydrogenated coronene dominates over direct H_2 loss induced by UV photodestruction.

Unified Astronomy Thesaurus concepts: Astrochemistry (75)

1. Introduction

Polycyclic aromatic hydrocarbons (PAHs) in different charge and hydrogenation states are thought to be an important constituent of the interstellar medium (ISM). The PAH hypothesis was proposed more than 35 years ago to interpret the so-called Unidentified Infrared Bands, a set of emission bands observed near 3.3, 6.2, 7.7, 8.6, 11.3, and 12.7 μm in many dusty environments (Leger & Puget 1984; Allamandola et al. 1985). PAHs have also been proposed as being responsible for the diffuse interstellar absorption bands (Bréchignac & Pino 1999; Biennier et al. 2003; Kokkin et al. 2008). For a review of the spectroscopic properties of PAHs and their role in the physics and chemistry of interstellar and circumstellar environments, see Tielens (2008, 2013) and Cherchneff (2011).

The general consensus is that interstellar H_2 forms efficiently *via* the recombination of atomic hydrogen on the surfaces of dust grains. Laboratory experiments employing appropriate grain analogs have indicated that this process occurs on a variety of dust grain surfaces such as silicates, carbonaceous materials, and water ice (Pirronello et al. 1997, 1999; Manicò et al. 2001; Hornekær et al. 2003). In addition, PAHs have also been proposed to provide catalytic sites for the formation of H_2. However, the reactions between physisorbed H atoms are efficient only for surface temperatures below 20 K. In environments with higher grain temperatures, such as photodissociation regions (PDRs), other routes to molecular hydrogen formation must be considered, as desorption of H atoms from weakly bound physisorbed sites is fast and recombination cannot take place (Vidali et al. 2005). Hydrogen atoms must be in more tightly bound states such as chemisorption states on PAHs, graphite, and highly defected surfaces (Habart et al. 2003, 2004; Cazaux & Tielens 2004; Cuppen & Herbst 2005; Hornekær et al. 2006a, 2006b). A recent article by Wakelam et al. (2017) reviews H_2 formation on interstellar dust grains in a variety of interstellar environments.

The link between PAHs and H_2 formation was highlighted by Habart et al. (2003), who observed a strong correlation between PAH and H_2 emission in the ρ Ophiuchi molecular cloud (PDRs). This led them to propose that PAHs can catalyze H_2 formation, although the Langmuir–Hinshelwood mechanism cannot explain their formation under the conditions prevalent in PDRs (Habart et al. 2004).

Theoretical and experimental studies have indicated several processes for H_2 formation on PAHs: (i) abstraction of edge H atoms of PAH cations by incoming H atoms (Cassam et al. 1994); (ii) addition of an H atom to an edge site of a PAH cation and the successive abstraction of the excess H atom by a second incoming H atom (Bauschlicher 1998). This mechanism should proceed, with a low energy barrier, also in the case of neutral PAHs (Rauls & Hornekær 2008); (iii) dissociative recombination of an hydrogenated cation with an electron (Le Page et al. 2009); (iv) H_2 ejection from a CH_2 aliphatic group of excited protonated PAHs (Szczepanski et al. 2011); (v) ultraviolet (UV) irradiation of hydrogenated neutral PAHs (Fu et al. 2012); (vi) photofragmentation of PAH cations (Castellanos et al. 2018).

In our previous experimental studies, we demonstrated the formation of highly superhydrogenated coronene using mass spectrometry (Thrower et al. 2012) and showed, using infrared (IR) spectroscopy, that molecular H_2 is formed through abstraction reactions from the exposure of hydrogenated coronene to atomic H (Mennella et al. 2012). D atoms were used in the above experiments to distinguish from the already attached H atoms on coronene molecules. Based on these experimental studies, we proposed that superhydrogenated neutral PAHs can catalyze H_2 formation under interstellar conditions.

Hydrogenation is the necessary condition for the formation of molecular hydrogen on neutral PAHs, providing the necessary degree of superhydrogenation for H_2 formation through abstraction to be efficient. In this context knowledge of the UV photodehydrogenation cross section for superhydrogenated PAHs is important in order to be able to estimate the degree of hydrogenation of PAHs under PDR and general ISM conditions. The present study is a natural extension of the

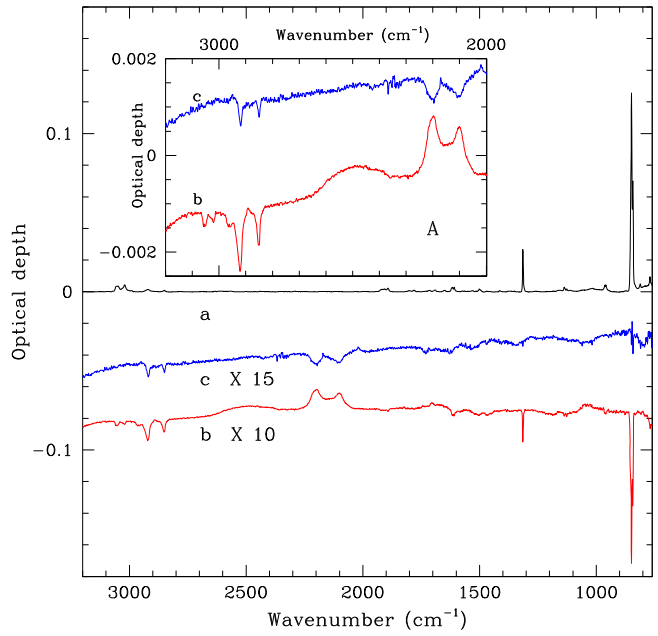

Figure 1. IR spectrum of COR03 film (a), after hydrogenation through exposure to 3.4×10^{18} D atoms cm^{-2} (b) and subsequent UV irradiation with 1.2×10^{19} photons cm^{-2} (c). The spectrum of the hydrogenated sample is shown after subtraction of the initial spectrum, while the spectrum after UV irradiation is shown after the subtraction of that of hydrogenated coronene. The difference spectra are offset for clarity. Inset A: the traces *b* and *c* are zoomed in the region where C–H and C–D stretching bands fall.

previous study and we report the IR spectral evolution of superhydrogenated coronene films exposed to UV photons.

2. Experiments and Results

The superhydrogenated coronene samples considered in the present study have been prepared in two phases. At first, samples were prepared in an ultrahigh vacuum chamber with a base pressure of $<1 \times 10^{-9}$ mbar. Coronene powder (Sigma-Aldrich; 99% purity) was heated in a thermal evaporation source to 185 °C and subsequently molecules were deposited on KBr substrates, located *ca.* 3 cm from the source. A deposition rate of 0.6 Å s^{-1} was determined with a quartz crystal microbalance at the substrate position. The resulting samples are compact films of coronene with film thicknesses of 100, 120, and 140 nm for the COR01, COR02, and COR03 samples, respectively. The IR spectrum of the COR03 sample is shown in Figure 1. In addition to the vibrational modes of coronene, the two weak bands at 2925 and 2850 cm^{-1}, are attributed to hydrocarbon contamination arising from air exposure during transfer of the samples. The contaminant features are also present in the spectrum of a blank KBr substrate used as a reference. The second phase of the sample preparation was performed in a vacuum chamber with a base pressure of $\sim 2 \times 10^{-8}$ mbar. Coronene films were exposed to an atomic deuterium beam produced by microwave-excited dissociation of molecular deuterium (99.96% purity) at room temperature. D atoms in the beam have a Maxwellian velocity distribution corresponding to 300 K (Mennella 2006). The films were irradiated with a fluence of 3.4×10^{18} D atoms cm^{-2}. The resulting intensity decrease of the coronene IR bands and the simultaneous increase in the intensity of the sp^3 C–D asymmetric and symmetric stretching modes of the CD_2 group at 2205 and 2100 cm^{-1}, respectively, (see trace b in the inset to Figure 1) are evidence for the hydrogenation of coronene. For a D atom fluence similar to that used in the present experiment, a coronene monolayer on graphite was driven toward a fully superdeuterated state with a mass distribution peaking at $C_{24}D_{35}$ as demonstrated by Skov et al. (2014) using mass spectrometry measurements. In the present experiment, we expect a similar degree of superhydrogenation in the first few layers of the coronene multilayer films, possibly decreasing with depth. This is testified by the variation of C=C stretch doublet at around 1600 cm^{-1}, although the exact degree of superhydrogenation cannot be estimated using IR spectroscopy (Mennella et al. 2012). Note that the intensity variations in the infrared spectrum are small with respect to the initial band intensity, consistent with D atoms only being able to interact with the superficial layers of coronene films, due to the compact nature of the films. In fact, the integrated optical depth values of the C–D stretching mode of the CD_2 group are similar and almost independent of the initial film thickness. The values for COR1, COR2, and COR3 films are, respectively, 0.117, 0.130, and 0.134 cm^{-1} with an average of 0.127 cm^{-1}. Using this average value, we have evaluated the penetration depth of the D atoms, d_D, through the following relation:

$$\int_{\text{band}} \Delta\tau(\nu)d\nu = NA = \frac{\rho\, d_D\, N_A}{m} A \qquad (1)$$

where N is the column density, A is the integrated band strength of aliphatic C–D bonds, and N_A is Avogadro's number. The parameters ρ and m are the density and the molecular weight, respectively. As a first approximation, we adopted the coronene bulk density $\rho = 1.371$ g cm^{-3} and $m = 360$ g mol^{-1} for fully superdeuterated coronene film. From the band strength data reported for three different aliphatic hydrocarbons by d'Hendecourt & Allamandola (1986), we obtained an average value of the band strength of 3.7×10^{-18} cm per C–H bond of the CH_2 group. The band strength of the aliphatic C–D bond was found to be a factor of 1.55 times lower than that of aliphatic C–H bond (Grishko & Duley 2002). Using these values we obtain a value of $d_D = 6.4$ nm for a fully superdeuterated coronene (36 C–D bonds).

A decrease of the sp^3 C–H stretching bands is also observed after D atom exposure. This is attributed to deuteration of contaminant hydrocarbon molecules. This conclusion is supported by experiments using blank KBr substrate where a similar intensity decrease of the aliphatic C–H stretching bands is observed during D atom irradiation. The contribution to the band intensity of the C–D stretching band is at most 12%. For a detailed discussion of the IR spectral variations induced by the D atom interaction with coronene, see Mennella et al. (2012).

UV irradiation of the superhydrogenated coronene films was carried out in the same vacuum chamber as during the second phase of the sample preparation. The IR spectral evolution of the samples during irradiation was studied with a resolution of 2 cm^{-1}. The UV source of the apparatus is a microwave-excited hydrogen flow discharge lamp. The source was operated at a hydrogen pressure of 0.5 mbar. Under these conditions Lyα (10.2 eV) emission accounts for 97% of the total UV emission of the source (Mennella et al. 2006). During sample irradiation, the UV flux (fluence) was monitored by measuring the current (charge) generated by the photoelectric effect on a platinum wire inserted between the source and the sample. Details on the calibration of the wire sensor and on the

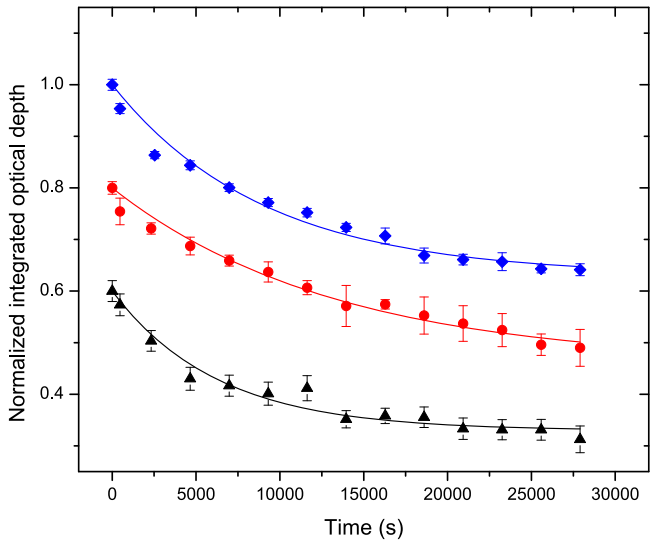

Figure 2. Evolution of the normalized band integrated optical depth of the C–D stretching modes of the CD_2 group with UV irradiation time for hydrogenated COR01 (black triangles), COR02 (red circles), and COR3 (blue diamonds) films. The data in red and black are offset in the ordinate by −0.2 and −0.4, respectively, for the sake of clarity. The best fit to the data of the relation $ae^{-Rt} + b$ is also shown (see Appendix B for details).

measurement of the flux at the sample position are given in Mennella (2006).

Exposure of superhydrogenated coronene films to Lyα photons results in an intensity decrease of the sp^3 asymmetric and symmetric stretching modes of the CD_2 group (see trace c in the inset to Figure 1). A very weak intensity decrease of the two most intense coronene bands, the C–H out of plane doublet at 849 and 843 cm^{-1} and the C–H in plane mode at 1314 cm^{-1}, is also observed. The intensity decrease of these bands could be due to the photoprocessing that determines the loss of H/H_2 in pristine coronene films underlying the superhydrogenated layers. To gain further insight into this, dedicated experiments focusing on the UV irradiation of pure coronene films would be useful. We have derived the mean free path of UV photons, d_{UV}, through the coronene films from the absorption coefficient α as $d_{UV} = 1/\alpha = 1/\sigma n$ where σ is the UV photoabsorption cross section of superhydrogenated coronene and n is the number of coronene molecules per unit volume. For 10.2 eV photons, we calculated the absorption cross section of fully superhydrogenated coronene as 1.9×10^{-16} cm^2 (see Appendix A). We then obtained $d_{UV} = 23$ nm. Note that, we used the bulk density of coronene to evaluate n. However, upon complete hydrogenation coronene molecules are distorted and the bulk density should be lower and the estimated d_{UV} should therefore be considered a lower limit. Nevertheless, the estimated penetration depth of UV photons is 3 times larger than that of the D atoms.

The evolution of the normalized integrated optical depth of the C–D modes of superhydrogenated coronene with UV irradiation time is reported in Figure 2, along with best fits to the experimental data. The cross section of UV photodestruction of the C–D bonds, $\sigma_{UV} = (8 \pm 2) \times 10^{-20}$ cm^2, was estimated from the best-fit parameters for the three films investigated (for more details on the fitting procedure see Appendix B).

3. Discussion

As already reported in the previous section, coronene molecules in the first few layers of the film should be highly superhydrogenated for the considered D atom fluences. Superhydrogenation is the result of a series of addition and exchange reactions involving D atoms at the outer and inner edge carbon sites of coronene, transforming carbon hybridization from aromatic sp^2 to aliphatic sp^3 (Mennella et al. 2012). Hence, fully superhydrogenated coronene is purely aliphatic in nature. The absence of the $\Pi^\star \leftarrow \Pi$ transition in the UV absorption spectrum also highlights the aliphatic nature of fully superhydrogenated coronene (see Appendix A).

The photoabsorption spectrum calculated for superhydrogenated coronene reveals that 10.2 eV photons lie at the low energy wing of the broad peak due to the $\sigma^\star \leftarrow \sigma$ transition (see Appendix A). Upon 10.2 eV photon irradiation, electrons in the C–D bonds are excited to an anti-bonding orbital, resulting in a D atom loss because the dissociation energy of aliphatic C–D bond is lower. The excitation might be extended to more than one bond, resulting in the loss of a D_2 molecule with a smaller ejection probability than that for D atom loss. The decrease of the band intensity of the CD_2 groups is a clear evidence that UV photons are able to induce photodestruction. However, with infrared spectroscopy we cannot estimate the exact contribution of the two loss processes even if we expect D atom loss to be dominant (Boschman et al. 2015). We can compare the estimated cross section with that obtained for other aliphatic compounds. In fact, our cross section compares well with that estimated for UV destruction cross section of C–H bonds in amorphous hydrogenated carbon grains and hydrocarbon molecules (Mennella et al. 2001; Muñoz Caro et al. 2001).

The effect of UV photons on superhydrogenated PAHs have been studied with a limited number of theoretical studies. To the best of our knowledge, we have found just a recent experimental study where vacuum ultraviolet (VUV)-induced unimolecular dissociation of superhydrogenated tetralin ions result in loss of small hydrocarbons rather than H atoms (Diedhiou et al. 2019). The existing experimental works mainly concern the photostability of superhydrogenated PAH cations under X-ray irradiation. There are contrasting results suggesting that the presence of additional H atoms acts either as a buffer against photofragmentation or leads to the weakening of the carbon backbone, favoring the fragmentation (Reitsma et al. 2014; Gatchell et al. 2015; Wolf et al. 2016). Concerning UV photons, theoretical works by Boschman et al. (2015) considered all the superhydrogenation states of coronene starting from one extra H atom up to the fully superhydrogenated molecule and computed the rate for H atom loss to be an order of magnitude higher that that for the ejection of a H_2 molecule. The rates were found to be equal for all hydrogenation states and therefore independent of the degree of superhydrogenation. However, we note that Jensen et al. (2019) demonstrated, through a combination of mass spectrometry and density functional theory (DFT) calculations, that coronene with specific hydrogenation degrees of 2, 10, 14, 18, and 24 extra H atoms are relatively more stable than the others. Therefore, one would expect a variation in the rate depending on the degree of superhydrogenation. Nevertheless, in order to compare our experimental work with the theoretical result of Boschman et al. (2015), we transformed their rates into the corresponding cross sections and obtained values of

2.6×10^{-17} cm^2 and 1.23×10^{-18} cm^2 for H atom and H_2 loss, respectively. Our experimental cross section of 8×10^{-20} cm^2 is two orders of magnitude lower than their values obtained for H atom loss.

It is worth noting that until now we have only discussed the effect of UV photons on a fully superhydrogenated PAH system. However, in space a PAH molecule may not be fully hydrogenated and, as a result, PAH molecules should retain their aromaticity to some extent. Therefore, the general effects of UV photons on PAHs and hydrogenated PAHs with a few extra H atoms are of interest. Recently, Andrews et al. (2016) considered superhydrogenated coronene with up to two extra H atoms and, based on DFT calculations, they also found that superhydrogenated coronene will preferentially lose H atoms rather than H_2 molecules. In addition, they found that the rate for H atom loss decreases with increasing size of superhydrogenated PAHs, i.e., coronene ($C_{24}H_{12}$) > circumcoronene ($C_{54}H_{18}$) > circumcircumcoronene ($C_{96}H_{24}$). The results of UV photon absorption were similar for neutral PAHs where coronene and other neutral PAHs containing less than 30–40 carbons would lose H atoms, whereas larger PAHs would remain unchanged as they relax through IR emission (Jochims et al. 1994). Recently, ionization was found to be the dominant process in PAH cations with up to ~50 carbon atoms when processed by VUV photons, whereas evidence for a hydrogen dissociation channel was found for smaller PAHs (Joblin et al. 2020). In any case, to evaluate the photodestruction cross section of superhydrogenated coronene with a few extra H atoms, as a first approximation, one can scale our experimental cross section values according to the corresponding degree of superhydrogenation.

4. Astrophysical Implications

There has been a lot of ongoing research to investigate how molecular H_2 can be efficiently formed in PDRs. PAHs in different charge and hydrogenation states can play an important role in this process. The catalytic role of superhydrogenated neutral coronene in H_2 formation has already been demonstrated through several laboratory experiments (Mennella et al. 2012). To determine the likely degree of superhydrogenation of PAHs under interstellar conditions, there is a need to evaluate the counteracting effect of UV photons because the hydrogenation degree in superhydrogenated PAHs will be determined by a balance between H-addition and H-loss through UV-induced photodestruction. We adopt the photodestruction cross section estimated for a superhydrogenated coronene film as a reference value to discuss the implication for H_2 formation in PDRs. Our cross section value suggests a lower rate of H atom loss than previously indicated by computational calculations. Consequently, this result would extend the regions inside PDRs where superhydrogenated coronene can survive and contribute to H_2 formation compared to those previously determined from the chemical models (Boschman et al. 2015; Andrews et al. 2016). It would also be possible to observe the infrared spectral features of superhydrogenated coronene in different regions of space at 3.51 and 3.56 μm as predicted by recent DFTs (Pla et al. 2020). Extensive kinetic models would be useful to incorporate the experimental results of both H-addition and UV photodestruction to estimate the degree of superhydrogenation of coronene as a model PAH under PDR conditions. However, such models are beyond the scope of the present Letter.

Another implication of our result concerns the evaluation of the contribution of superhydrogenated species to H_2 formation by interaction of UV photons and through abstraction by H atoms. With this in mind, we compare the ratio of the rates of the two processes to find out which one prevails. The ratio is given by

$$\frac{R_{\rm UV}}{R_{\rm H}} = \frac{\sigma_{\rm UV}\phi_{\rm UV}}{\sigma_{\rm H}\phi_{\rm H}}, \quad (2)$$

where R, σ and ϕ refer to the rates, cross sections, and fluxes of UV photons and H atoms. As discussed above, the photodestruction cross section of 8×10^{-20} cm^2 corresponds to H atom loss and, based on the theoretical result of Boschman et al. (2015), the corresponding cross section for direct H_2 loss should be an order of magnitude smaller, ca. 8×10^{-21} cm^2. On the other hand, the cross section for Eley–Rideal H_2 abstraction by H atoms, evaluated on similar superhydrogenated coronene films, is $\sigma_{\rm H} = 6 \times 10^{-18}$ cm^2 (Mennella et al. 2012). This results in a cross-section ratio of $\sigma_{\rm UV}/\sigma_{\rm H} = 1.3 \times 10^{-3}$. Concerning the evaluation of the flux ratio, we use the recent theoretical results presented by Andrews et al. (2016), who found that superhydrogenated coronene molecules can be present in PDRs at the 10%–15% level when the ratio of the UV field intensity to the H density ($n_{\rm H}$) is below 0.05 at a gas temperature of 500 K. This constraint corresponds to a flux ratio, $\phi_{\rm UV}/\phi_{\rm H} \lesssim 15$. Therefore, we obtain $R_{\rm UV}/R_{\rm H} \lesssim 2 \times 10^{-2}$, implying that, on superhydrogenated coronene, the rate of H_2 formation by the effect of UV photon irradiation is at least two orders of magnitude slower than H_2 formation through Eley–Rideal H_2 abstraction. This conclusion is in agreement with a recent experimental investigation involving coronene cations (Foley et al. 2018).

5. Conclusions

The present experimental study has provided the UV photodestruction cross section of small superhydrogenated PAHs. Our result suggests that small superhydrogenated PAHs can survive in more extended regions inside PDRs than previously determined. We also found that under physicochemical conditions expected in PDRs where small superhydrogenated PAHs can survive, H_2 formation through Eley–Rideal H abstraction prevails over H_2 loss induced by UV photodestruction.

This work has been supported by INAF research contracts and the Danish National Research Foundation through the Center of Excellence "InterCat" (grant agreement No. DNRF150).

Appendix A
Calculation of the UV Absorption Cross Section of the Fully Superhydrogenated Coronene

The electronic absorption spectra of fully superhydrogenated coronene have been obtained in the framework of time-dependent DFT (TD-DFT), following the same procedure used in Malloci et al. (2007). Among the many stereoisomers of $C_{24}H_{36}$, we chose the two extrema, namely the one in which all additional H atoms attached to C atoms in the central structure of coronene are on the same side, and the one in which

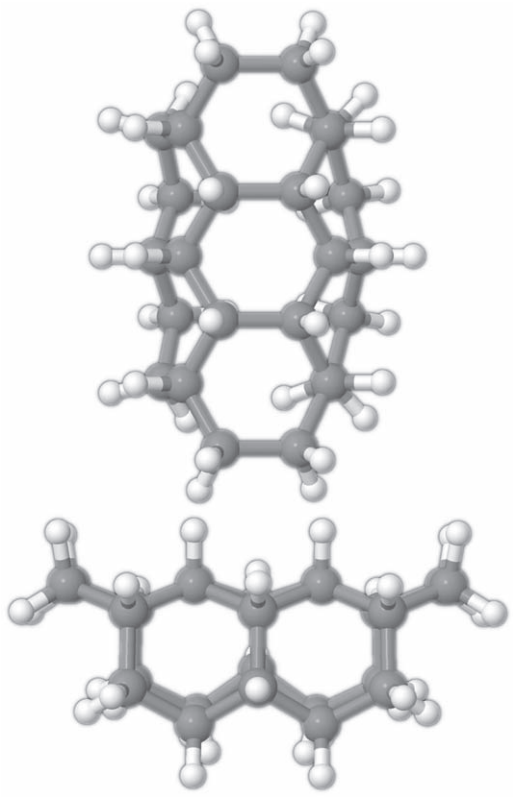

Figure 3. Structure of $C_{24}H_{36}$ with all H atoms on the same side, from two viewing angles.

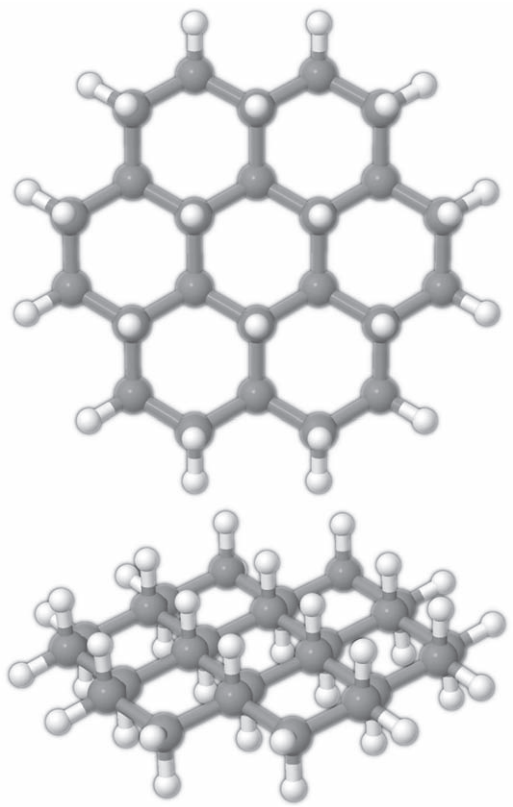

Figure 4. Structure of $C_{24}H_{36}$ with H atoms on alternating sides of the distorted carbon plane of coronene, from two viewing angles.

neighboring H atoms are always on opposite sides of the distorted carbon plane. Their structures are shown in Figures 3 and 4. The ground states of the two structures were optimized using DFT, in particular with the B3LYP hybrid exchange-correlation functional (Stephens et al. 1994) and the 6–31g(d,p) Gaussian basis set (Ditchfield et al. 1971), as implemented in the Gaussian16 quantum chemistry package (Frisch et al. 2016). These calculations were run on the Galileo supercomputer at CINECA.

After optimization, we used a TD-DFT simulation in real-time and real-space to obtain the response of the electrons to an applied instantaneous electric field, in the linear regime, keeping ion positions frozen. From the time-dependent electric dipole resulting from the simulation, the complex electric polarizability tensor was obtained *via* a numerical Fourier transform. The vertical electronic photoabsorption cross section is then proportional to the trace of the imaginary part of the polarizability tensor, at each frequency (Yabana & Bertsch 1999). Because the calculation was performed at the optimized geometries, with frozen ion configurations, it does not include any finer vibronic structure, and is completely independent of the isotopic masses of the component atoms. This means the results are identically applicable to any isotopomers of the same molecules, e.g., $C_{24}D_{36}$ as well as $C_{24}H_{36}$. These calculations were performed using the open-source Octopus quantum chemistry code (Marques et al. 2003). Octopus represents all wave functions using a discrete grid in a finite-size simulation box. Following calibration calculations performed in Joblin et al. (2020), we chose a simulation box composed of the union of spheres, each with a radius of 8 Å, centered on each atom of the molecule being studied, together with a grid spacing of 0.18 Å. For the TD-DFT simulations we used the simple LDA exchange-correlation functional, as this has been shown to provide an overall good match to experimental data on polycyclic aromatic hydrocarbons (Malloci et al. 2004; Joblin et al. 2020). The spectra obtained are shown in Figure 5, together with the spectrum of pristine coronene, taken from Malloci et al. (2007).

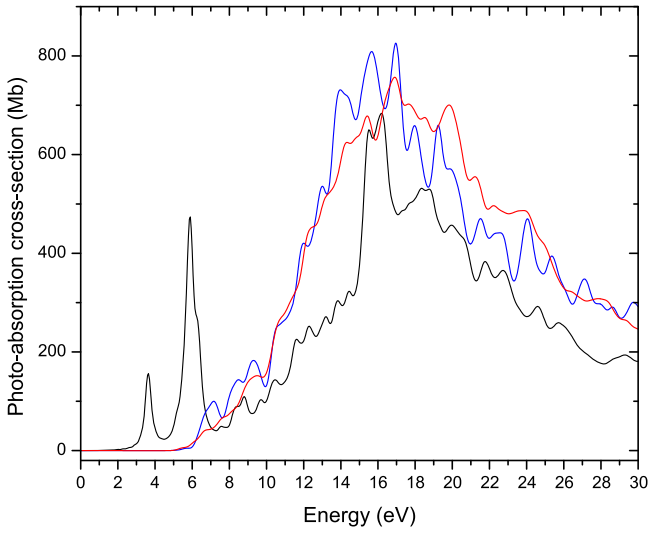

Figure 5. Comparison between the photoabsorption cross section for neutral coronene ($C_{24}H_{12}$, black line; Malloci et al. 2007) and for fully superhydrogenated coronene ($C_{24}H_{36}$, blue and red lines). All extra H atoms are either attached to one of the face of the molecule (red line) or at alternate faces (blue line).

It can be clearly seen that the $\pi^* \leftarrow \pi$ transitions of coronene are completely suppressed in both the fully superhydrogenated

Table 1
Fitting Parameters

Sample Name	Parameters		
	R s^{-1}	a	b
COR1	$(1.6 \pm 0.2) \times 10^{-4}$	0.27 ± 0.01	0.73 ± 0.01
COR2	$(7.5 \pm 1.3) \times 10^{-5}$	0.34 ± 0.02	0.66 ± 0.03
COR3	$(1.1 \pm 0.2) \times 10^{-4}$	0.37 ± 0.02	0.63 ± 0.02

molecules, while the overall envelope of the $\sigma^* \leftarrow \sigma$ transitions does not change much in shape, with a global enhancement in the hydrogenated species compared to coronene. This is intuitively expected, as with full superhydrogenation carbon bonds become fully aliphatic, and so do the molecular orbitals, i.e., there are no π, nor π^* orbitals left. On the other hand, there are more σ and σ^* orbitals available, enhancing corresponding transitions. It is also remarkable that while there are some spectral structure differences between the two $C_{24}H_{36}$ stereoisomers, the broad envelope is very nearly the same, in particular around the energy of the Lyα photons used for the UV irradiation. Therefore, we infer that the precise structure of the fully superhydrogenated coronene molecules is not likely to change much their photoabsorption rate around 10.2 eV.

Appendix B
Fitting Procedure for the Evaluation of Destruction Cross Section

Under the hypothesis of a first-order kinetic process, the destruction of aliphatic C–D bonds of fully superhydrogenated coronene by UV photons is given by

$$\tau_{CD}(t) = a\, e^{-Rt} \tag{B1}$$

where a is the band intensity for $t = 0$ and R is the destruction rate. Relation (B1) predicts a complete C–D bond destruction with time and the asymptotic value is zero, in agreement with the fact that UV photons have a mean free path longer than the layer of fully superhydrogenated coronene layer. However, the experimental trends of the $\tau_{CD}(t)$ suggests a non-zero asymptotic value. Therefore, Relation (B1) has been modified to reproduce the experimental data as follows:

$$\tau_{CD}(t) = a\, e^{-Rt} + b \tag{B2}$$

Relation (B2) provides a better representation of the experimental trends. The best fits to the experimental data are shown in Figure 2 and the fitting parameters are reported in Table 1. Actually, Relation (B2) describes a condition in which a C–D formation process able to counteract UV photodestruction is active. In fact, at a film temperature of 300 K, UV photolyzed D atoms can easily diffuse through the film and reform C–D bonds. Evidence for such a recombination was also found for aliphatic C–H bonds of hydrogenated carbon grains after ion irradiation (Mennella et al. 2003). The intensity of the IR aliphatic C–H band was reduced to ~5% of the initial value after irradiation by 30 keV He^+ at 12 K. After ion irradiation, at the end of warm up, the C–H band intensity increases to ~40% of the initial value as a consequence of thermal activated recombination of C–H bonds.

Determining the complete evolution of the number of C–D bonds would require a rigorous theoretical modeling which is beyond the scope of the present Letter. However, to get insight, we have considered as a first approximation a solution for the evolution of the bonds under the hypothesis of independent counteracting processes, i.e., formation by H atoms and destruction by energetic processing proposed by Mennella et al. (2003). Adapting their solution (13) to the present case we have

$$\tau'_{CD}(t) = \frac{R_{UV}}{R_D + R_{UV}}\, e^{-(R_D + R_{UV})t} + \frac{R_D}{R_D + R_{UV}} \tag{B3}$$

where $\tau'_{CD}(t)$ is the integrated band intensity normalized to the maximum number of hydrogenated C–D bonds and $\tau_{CD} = 1$ for $t = 0$ as in the case of the data reported in Figure 2. R_D and R_{UV} are the rates of D atom recombination and UV photodestruction, respectively. Comparing relations (B2) and (B3), one can see that R is the total rate and a, b are the corresponding fractional ratio of the two processes. From each set of best-fitting parameters reported in Table 1, we derived $\sigma_i = a_i R_{UV,i}/\phi$, $(i = 1, 2, 3)$ and the corresponding errors $(\Delta\sigma_i)$ by propagating the errors on a_i, $R_{UV,i}$ and ϕ. The experimental average value of the UV flux, ϕ, was 4.3×10^{14} photons $cm^{-2}\, s^{-1}$. The uncertainty in ϕ is ~20% (Mennella et al. 2006). Then, by taking the weighted average of σ_i, we obtained the value of $\sigma_{UV} = (8 \pm 2) \times 10^{-20}$ cm^2.

ORCID iDs

V. Mennella https://orcid.org/0000-0001-9525-895X
T. Suhasaria https://orcid.org/0000-0002-4755-4719
J. D. Thrower https://orcid.org/0000-0003-0974-8077

References

Allamandola, L. J., Tielens, A. G. G. M., & Barker, J. R. 1985, ApJL, 290, L25
Andrews, H., Candian, A., & Tielens, A. G. G. M. 2016, A&A, 595, A23
Bauschlicher, C. W., Jr. 1998, ApJL, 509, L125
Biennier, L., Salama, F., Allamandola, L. J., & Scherer, J. J. 2003, JChPh, 118, 7863
Boschman, L., Cazaux, S., Spaans, M., Hoekstra, R., & Schlathölter, T. 2015, A&A, 579, A72
Bréchignac, P., & Pino, T. 1999, A&A, 343, L49
Cassam-Chenaï, P., Pauzat, F., & Ellinger, Y. 1994, in AIP Conf. Proc. 312, Molecules and Grains in Space, ed. I. Nenner (Melville, NY: AIP), 543
Castellanos, P., Candian, A., Zhen, J., Linnartz, H., & Tielens, A. 2018, A&A, 616, A166
Cazaux, S., & Tielens, A. G. G. M. 2004, ApJ, 604, 222
Cherchneff, I. 2011, EAS, 46, 177
Cuppen, H. M., & Herbst, E. 2005, MNRAS, 361, 565
d'Hendecourt, L. B., & Allamandola, L. J. 1986, A&AS, 64, 453
Diedhiou, M., West, B. J., Bouwman, J., & Mayer, P. M. 2019, JPCA, 123, 10885
Ditchfield, R. H. W. J., Hehre, W. J., & Pople, J. A. 1971, JChPh, 54, 724
Foley, N., Cazaux, S., Egorov, D., et al. 2018, MNRAS, 479, 649
Frisch, M. J., Trucks, G. W., Schlegel, H. B., et al. 2016, Gaussian 16 Revision A 03, Gaussian Inc., Wallingford, CT https://gaussian.com/citation_a03/
Fu, Y., Szczepanski, J., & Polfer, N. C. 2012, ApJ, 744, 61
Gatchell, M., Stockett, M. H., de Ruette, N., et al. 2015, PhRvA, 92, 050702
Grishko, V. I., & Duley, W. W. 2002, ApJL, 583, L43
Habart, E., Boulanger, F., Verstraete, L., et al. 2003, A&A, 397, 623
Habart, E., Boulanger, F., Verstraete, L., Walmsley, C. M., & Pineau des Forêts, G. 2004, A&A, 414, 531
Hornekær, L., Baurichter, A., Petrunin, V. V., Field, D., & Luntz, A. C. 2003, Sci, 302, 1943
Hornekær, L., Rauls, E., Xu, W., et al. 2006a, PhRvL, 97, 186102
Hornekær, L., Šljivančanin, Ž., Xu, W., et al. 2006b, PhRvL, 96, 156104
Jensen, P. A., Leccese, M., Simonsen, F. D., et al. 2019, MNRAS, 486, 5492
Joblin, C., Wenzel, G., Castillo, S. R., et al. 2020, JChPh, 1412, 062002
Jochims, H. W., Ruhl, E., Baumgartel, H., Tobita, S., & Leach, S. 1994, ApJ, 420, 307

Kokkin, D. L., Troy, T. P., Nakajima, M., et al. 2008, ApJL, 681, L49
Le Page, V., Snow, T. P., & Bierbaum, V. M. 2009, ApJ, 704, 274
Leger, A., & Puget, J. L. 1984, A&A, 137, L5
Malloci, G., Joblin, C., & Mulas, G. 2007, CP, 332, 353
Malloci, G., Mulas, G., & Joblin, C. 2004, A&A, 426, 105
Manicò, G., Ragunì, G., Pirronello, V., Roser, J. E., & Vidali, G. 2001, ApJL, 548, L253
Marques, M. A. L., Castro, A., Bertsch, G. F., & Rubio, A. 2003, CoPhC, 151, 60
Mennella, V. 2006, ApJL, 647, L49
Mennella, V., Baratta, G. A., Esposito, A., Ferini, G., & Pendleton, Y. J. 2003, ApJ, 587, 727
Mennella, V., Baratta, G. A., Palumbo, M. E., & Bergin, E. A. 2006, ApJ, 643, 923
Mennella, V., Caro, G. M., Ruiterkamp, R., et al. 2001, A&A, 367, 355
Mennella, V., Hornekær, L., Thrower, J., & Accolla, M. 2012, ApJL, 745, L2
Muñoz Caro, G. M., Ruiterkamp, R., Schutte, W. A., Greenberg, J. M., & Mennella, V. 2001, A&A, 367, 347
Pirronello, V., Biham, O., Liu, C., Shen, L., & Vidali, G. 1997, ApJL, 483, L131
Pirronello, V., Liu, C., Roser, J. E., & Vidali, G. 1999, A&A, 344, 681
Pla, P., Wang, Y., Martín, F., & Alcamí, M. 2020, ApJ, 899, 18
Rauls, E., & Hornekær, L. 2008, ApJ, 679, 531
Reitsma, G., Boschman, L., Deuzeman, M. J., et al. 2014, PhRvL, 113, 053002
Skov, A. L., Thrower, J. D., & Hornekær, L. 2014, FaDi, 168, 223
Stephens, P. J., Devlin, F. J., Chabalowski, C. F., & Frisch, M. J. 1994, JPCA, 98, 11623
Szczepanski, J., Oomens, J., Steill, J. D., & Vala, M. T. 2011, ApJ, 727, 12
Thrower, J. D., Jørgensen, B., Friis, E. E., et al. 2012, ApJ, 752, 3
Tielens, A. G. G. M. 2008, ARA&A, 46, 289
Tielens, A. G. G. M. 2013, RvMP, 85, 1021
Vidali, G., Roser, J., Manicó, G., et al. 2005, JChPh, 6, 36
Wakelam, V., Bron, E., Cazaux, S., et al. 2017, MolAs, 9, 1
Wolf, M., Kiefer, H. V., Langeland, J., et al. 2016, ApJ, 832, 24
Yabana, K., & Bertsch, G. F. 1999, IJQC, 75, 55